ADSORPTION OF PYRENE FROM AQUEOUS SOLUTIONS ONTO SEPIOLITE

EYÜP SABAH[1]* AND SABEHA OUKI[2]

[1]Department of Mining Engineering, Faculty of Engineering, Afyon Kocatepe University, 03200 Afyonkarahisar, Turkey
[2]Department of Civil and Environmental Engineering, Faculty of Engineering and Physical Sciences, University of Surrey, Guildford, UK

Abstract—Polycyclic aromatic hydrocarbons (PAHs) are a large class of organic compounds which are commonly mentioned and have been shown to be highly carcinogenic and to persist in the environment for many years. An inexpensive remediation method has yet to be found, so the current study was undertaken to test the use of sepiolite, a fibrous clay mineral, as a potentially inexpensive and effective solid-phase adsorbent for sequestering PAHs. Pyrene was chosen as a model PAH due to the specific volatility, miscibility, and relatively soluble properties of the compound. A sepiolite of Turkish origin was then investigated to explore its potential to adsorb hydrophobic organic compounds from aqueous solution. The microstructure and morphology of the sepiolite were characterized using elemental analysis, X-ray diffractometry (XRD), Fourier-transform infrared (FTIR) spectroscopy, field emission scanning electron microscopy (FE-SEM), and specific surface area from N_2 adsorption isotherms. The pyrene adsorption isotherms were closely fitted to the Langmuir model and the coefficients of determination (R^2) were higher than 0.999. The results indicated that the high affinity of pyrene for sepiolite surfaces was dominated by the structural channels and the large number of Si-OH groups located on the basal surfaces. The intracrystalline interactions of pyrene with the sepiolite were, however, more favorable than pyrene interactions with sepiolite surface Si-OH groups, which can react directly with pyrene to form true covalent bonds (chemical interactions). Finally, the FE-SEM images initially revealed that, after sepiolite was loaded with adsorbed pyrene, a fairly straight and rigid arrangement of fibers occurred due to the aggregation of laths to form rods and the increased amounts of adsorbed pyrene.

Key Words—Adsorption, Pyrene, Sepiolite, Sepiolite Surface Channels, Si-OH Groups.

INTRODUCTION

Polycyclic aromatic hydrocarbons (PAHs) are one of the most widespread and persistent organic pollutants in terrestrial, atmospheric, and aquatic environments. They contain two or more fused aromatic rings made up of C and H atoms and derive mainly from anthropogenic sources, which include the combustion of fossil fuels, waste incineration, coke and asphalt production, oil refining, aluminum production, and many other industrial activities. PAHs are chemically inert, soluble in many organic solvents, and highly lipophilic. Their behavior and biological effects are, therefore, rather variable in the environment (Dowaidar *et al.*, 2007). Due to the stable poly-condensed aromatic structure, PAHs can be transported over long distances in water and be widely distributed in aquatic ecosystems (Dai *et al.*, 2011). Many rivers and lakes around the world are reported to be polluted by PAHs to different degrees and PAH concentrations in waters have reached the level of several micrograms per liter (Malik, 2004; Cho *et al.*, 2009; Sun *et al.*, 2009).

PAHs are often resistant to biological degradation due to the high-molecular weight and are not efficiently and/or economically removed from polluted water and waste-water by conventional physicochemical methods, such as coagulation, flocculation, filtration, ozonation, reverse osmosis, and oxidation processes. Adsorption processes by solids are, however, an effective method for the removal of PAHs from wastewater (domestic and/or industrial). Activated C is believed to be the most effective and widely used conventional adsorbent in this field, but its high cost and difficult regeneration are clear disadvantages (Ania *et al.*, 2007; Valderrama *et al.*, 2008; Pal, 2012; Marchal *et al.*, 2013). Other adsorbents, such as zeolites, resins, clays, carbon nanoporous materials, soils, and organic-free hydrophilic minerals like silica, alumina, talc, fly ash, and solid residues from agricultural activities like ash waste and pine bark have also been employed to successfully remove PAHs (Chang *et al.*, 2004; Sun *et al.*, 2009; Lemić *et al.*, 2007; Crisafully *et al.*, 2008; Anbia, and Moradi, 2009; Hall *et al.*, 2009; Sener and Zyilmaz, 2010; Li *et al.*, 2010; Perez-Gregorio *et al.*, 2010; Dai *et al.*, 2011; Vidal *et al.*, 2011). Natural materials, such as clays, are most suitable given the availability, low cost, environmental stability, and the high adsorptive and ion-exchange properties. With specific reference to pyrene, several studies have measured its adsorption from dilute aqueous solutions by inorganic and organic materials (Morozzi, and Scardazza, 1998; Kirso *et al.*, 2000; Irha, 2000; Ramirez and Cutright, 2001; Laegdsmand *et al.*, 2004; Hur and Schlautman, 2006; Owabor *et al.*, 2010; Teixeira *et al.*, 2011; Zhang *et al.*, 2009; Yakout and Daifullah, 2013).

* E-mail address of corresponding author:
esabah@aku.edu.tr

The fibrous clay mineral, sepiolite, with structural pores/channels and silanol surface-active adsorption sites have molecular-sieving abilities which enables this unique mineral to be used as a potential alternative for conventional sorbents. This is due to the relatively high surface area which allows a high adsorption capacity for the adsorption of a great variety of compounds in a very cost effective fashion. The three-dimensional microcrystalline structure of sepiolite is rigid during adsorption as no changes in the dimensions of particles occurs. This rigidity also implies that each particle maintains mechanical strength even when saturated with liquids (Alvarez et al., 2011). In contrast with bentonitic (smectite-rich) clays, these fibrous clays are non-swelling, and the structure is stable even in systems with high salt concentrations. Because of the elongate shape, sepiolite minerals are excellent suspension aids in systems with high electrolyte contents, which cause smectite particles to flocculate. Sepiolite particles do not flocculate because the elongate crystals hinder settling (Murray, 2007). In the past two decades, sepiolite and different kinds of surfactant (e.g. quaternary amines, organic dyes, silanes) modified sepiolites were applied to remove heavy metals and some polar organic pollutants, such as basic dyes, from waste effluents. However, no specific and systematic studies have been reported on the interactions between pyrene and sepiolite except the study by Cobas et al. (2014) which investigated the ability of sepiolite to remove model PAHs, such as phenanthrene and pyrene. In our study, the interactions between sepiolite and pyrene have been investigated in detail by characterizing the structure of sepiolite through Fourier-transform infrared spectroscopy (FTIR), field emission scanning electron microscopy (FE-SEM), specific surface area, pore size, and pore volume before and after adsorption studies. In the Cobas et al. (2014) study thermodynamic parameters of pyrene adsorption onto sepiolite from adsorption experiments were only determined at 298 K, but adsorption experiments were performed at 298, 313, and 328 K in the present study.

The aim of this study was to evaluate the potential of sepiolite for pyrene adsorption and to understand the adsorption mechanisms involved using adsorption, thermodynamics, and surface analysis data.

EXPERIMENTAL

Materials

The sepiolite samples used in the experiments were natural, non-swelling fibrous clays from Sivrihisar-Kurtşeyh, which occur in the upper Sakarya Section of the Central Anatolian Neogene Basin southeast of Eskisehir, Turkey.

Pyrene (98%; Sigma-Aldrich Chemical Co., Gillingham, UK) was selected as the PAH probe (Table 1) to determine equilibrium adsorption isotherm parameters. The inorganic chemicals, such as HCl, NaOH, and methanol, were used to adjust the pH, extract humic acid, and prepare pyrene solutions and were obtained from Fisher Scientific (Fair Lawn, New Jersey, USA). All solutions were prepared using de-ionized water with a resistivity of 15.3 MΩ-cm and were stored at room temperature (20±2ºC). The samples containing pyrene were stored in the dark due to the aromatic structure, which strongly adsorbs ultraviolet light in the UV-A (λ = 320−400 nm) and UV-B (λ = 290−320 nm) range of natural sunlight (Newsted and Giesy, 1987).

Methods

The raw sepiolite sample was first crushed by a two-stage crushing procedure using a laboratory jaw and roll crusher to prepare the <2 mm samples as a starting material. The sepiolite sample was then dry ground in a vibrating ball mill for a short grinding time of 25 min to avoid structural deformation (Vučelić et al., 2002; Kojdecki et al., 2005). The particle size distribution of the ground samples was analyzed by a technique based on laser light scattering using a Malvern Mastersizer 2000 (Malvern Instruments, Ltd., Malvern, UK).

The bulk density of the sepiolite sample was measured using a Haver bulk density tester (Haver & Boecker, Oelde, Germany) according to the EN 1097-3 (1998) standard method. The BET surface area, pore volume, and average pore diameter of the sepiolite sample were determined using a Quantachrome surface area analyzer (Quantachrome, Ltd., Hook, Wales, UK) using N_2 gas adsorption at −196ºC. Before each measurement, all samples were outgassed for 10 h by heating at 60ºC under vacuum.

Table 1. Structural characteristics and selected properties of pyrene.

PAH	Structure	Formula	Molecular weight (g/mol)	Molecular dimension ($\mathring{A} \times \mathring{A} \times \mathring{A}$)	Molecular area (nm^2)	Water solubility at 25ºC (mg/mL)	Log K_{OW}
Pyrene		$C_{16}H_{10}$	202.25	[a]9.2 (kinetic diameter [c]7.0 $\mathring{A}$)	[b]1.07	0.135	[a]5.18

[a]Yuan et al. (2010); [b]Wang et al. (2014); [c]Iu and Thomas (1990)

The sepiolite sample was chemically analyzed with an X-ray fluorescence (XRF) spectrometer (ZSX Primus II XRF, Rigaku Corporation, Tokyo, Japan). X-ray powder diffraction patterns (XRD) of the sepiolite samples were measured using a Panalytical X Pert Pro MPD (PANalytical B.V., Almelo, The Netherlands) X-ray diffractometer. A JEOL JSM-7100F field emission scanning electron microscope (FE-SEM) equipped with a Link System energy dispersive X-ray (EDX) micro-analyser (JEOL, Inc., Peabody, Massachusetts, USA) was used to observe the textural features of the natural sepiolite and the pyrene-adsorbed sepiolite sample at low (2 mg/L) and high (4 mg/L) pyrene concentrations. The samples were coated with a gold/carbon film. FTIR spectra were recorded using an Agilent Cary 640 FTIR (Agilent Technologies, Inc., Santa Clara, California, USA) high-performance spectrometer using attenuated total reflectance (ATR) and diffuse reflection (DR) for rapid characterization of the natural sepiolite and sepiolite samples with adsorbed pyrene. The spectra were measured in the spectral range from 4000 to 400 cm^{-1} (32 scans, 4 cm^{-1} resolution).

A concentrated primary stock solution with 1,000 mg/L pyrene was prepared by completely dissolving an appropriate amount of pyrene in methanol (Fisher Scientific, Fair Lawn, New Jersey, USA). A 2.5-mL aliquot of this concentrated stock solution was diluted with methanol to 250 mL to give a 10 mg/L pyrene dilute stock solution. The dilute stock solution was further diluted with deionized water to prepare 50 mL of 50, 100, 200, 400, 600, and 800 µg/L pyrene solutions for calibrating the GC/MS. To obtain the initial pyrene concentrations that were chosen based on pyrene solubility in water, a 10 mg/L stock solution was serially diluted with deionized water to produce pyrene concentrations that ranged from 1 mg/L to 6 mg/L.

The pyrene adsorption experiments were conducted using <2 mm natural sepiolite samples in 40-mL glass bottles with Teflon-lined screw caps at the natural pH of the samples. Because the pH range was not a determining factor for pyrene removal, solutions without pH adjustment were used in all the batch adsorption experiments. Several studies (Paolis and Kukkonen, 1997; Zeledón-Toruno *et al.*, 2007) showed that PAHs with higher molecular weights and more C=C bonds (*e.g.* pyrene, benzo(k)fluoranthene, benzo(a)pyrene, and benzo(ghi)-perylene) are less affected by pH during adsorption. This is due to the fact that PAHs are chemically inert compounds with bond linkages that provide chemical stability. These compounds do not have ionizable groups that can be influenced by solution pH.

A 0.01-g sepiolite sample was mixed in 20 mL of pyrene solution with a solid to liquid ratio of 0.0005. In order to successfully assume that external diffusion limitations were negligible, the bottles were shaken at 250 rpm at room temperature and 25, 40, and 55ºC for 2 h on an orbital shaker-incubator to decide whether the

adsorption process was exothermic or endothermic (Sabah and Çelik, 2002; Sabah *et al.*, 2002). After centrifugation at 482×g for 10 min using a Heraeus Megafuge 16R centrifuge (Thermo Fisher Scientific, Waltham, Massachusetts, USA) and the supernatant solutions were filtered through 0.45 µm membrane filters (Millipore, Watford Hertfordshire, UK). A 0.5-mL aliquot of the clear supernatant was removed, after which the equilibrium concentration of pyrene was determined using a PerkinElmer Clarus 500 gas chromatograph (GC) coupled with a PerkinElmer Clarus 560 D mass spectrometer detector and an integrated liquid auto sampler (PerkinElmer, Inc, Shelton, Connecticut, USA). The GC temperature was programmed from an initial 50ºC with a 5ºC/min increase rate to a maximum temperature of 310ºC and a final holding time of 15 min. Helium was used as the carrier gas at a flow rate of 1 mL/min. A 1.0-µL aliquot of the extract was injected into the GC while the injector port was held at 280ºC and operated in splitless mode. Control (blank) experiments with no sepiolite present were conducted for each pyrene concentration level. Losses of pyrene by photochemical decomposition, volatilization, and sorption to the glass bottles and membrane filter were found to be negligible. In all cases, the equilibrium adsorption capacity after 2 h was calculated based on the differences in pyrene concentrations before and after the experiment according to the following equation 1:

$$q_e = \frac{(C_i - C_e)V}{W} \quad (1)$$

where C_i and C_e are the liquid phase initial and equilibrium concentrations of the pyrene in solution (mg/L), V (L) is the volume of the solution, and W (g) is the mass of the sepiolite.

The applicability of the isotherm models to quantify adsorption was compared by judging the correlation coefficients, R^2. The linear forms of the Langmuir and Freundlich equations are given in equations 2 and 3, respectively.

$$\frac{C_e}{q_e} = \frac{1}{q_m}C_e + \frac{1}{K_L q_m} \quad (2)$$

$$\ln q_e = \ln K_F + 1/n \ln C_e \quad (3)$$

where q_e is the amount of pyrene adsorbed per gram of sepiolite (mg/g), C_e is the equilibrium concentration of pyrene (mg/L), q_m is the maximum adsorption capacity at monolayer coverage (mg/g), K_L is the Langmuir adsorption equilibrium constant (L/mg) related to the affinity between the sepiolite and pyrene. In equation 3, n is a constant that depicts the adsorption intensity or surface heterogeneity with adsorption becoming more heterogeneous and more favorable at n values >1 and with an increase to ≈ 10, K_F is a Freundlich constant that represents the adsorption capacity (L/mg) and also

Table 2. Characteristics of the raw sepiolite.

Composition %-M	SiO$_2$ 46.40	Al$_2$O$_3$ 0.93	Fe$_2$O$_3$ 0.38	CaO 6.01	MgO 24.10	Na$_2$O 0.25	K$_2$O 0.54	TiO$_2$ 0.06	P$_2$O$_5$ 0.01	SrO$_2$ 0.08	SO$_3$ 0.08	F 1.51	LOI 19.67
Color	Brown												
Moisture (%)	10												
Density (g/cm^3)	2.33												
Apparent bulk density (g/L)	304.2												
BET Surface area (m^2/g)	358												
Mean pore diameter (Å)	47.2												
Total pore volume (cm^3/g)	0.559												
Particle size													
% less than 120.2 μm	100												
% less than 19.2 μm	50												

can be defined as an adsorption or distribution coefficient, which describes the amount of pyrene that adsorbs to sepiolite for a unit equilibrium pyrene concentration (Haghseresht and Lu, 1998; Öztürk and Bektas, 2004).

The data obtained from adsorption isotherm models can be conveniently used to determine such thermodynamic parameters as free energy of adsorption (ΔG^o_{ads}), enthalpy of adsorption (ΔH^o_{ads}), and the change in standard entropy (ΔS^o_{ads}). These parameters were evaluated using the following equation:

$$K_d = \frac{q_e}{C_e} \qquad (4)$$

where K_d (L/mol) is the sorption distribution coefficient. The K_d values were plugged into equation 5 to determine the free energy of the sorption process at different temperatures.

$$\Delta G^o_{ads} = -RT\ln K_d \qquad (5)$$

where ΔG^o_{ads} is the free energy of sorption (kJ/mol), T is the temperature in Kelvin, and R is the universal gas constant (8.31414 J/mol K).

The sorption distribution coefficient may be expressed in terms of enthalpy change (ΔH^o_{ads}) and entropy change (ΔS^o_{ads}) as a function of temperature as in equation 6.

$$\ln K_d = -\frac{\Delta H^o_{ads}}{RT} + \frac{\Delta S^o_{ads}}{RT} \qquad (6)$$

where ΔH^o_{ads} is the heat of adsorption (kJ/mol) and ΔS^o_{ads} is the standard entropy change (kJ/mol).

RESULTS AND DISCUSSION

Sepiolite characterization

The sepiolite used in this study was very low in Al and Fe content. The sepiolite sample was ground to <120.2 μm to produce an average particle size ($\bar{d}$) of 19.2 μm, whereas the density and bulk density were 2.33 g/cm^3 and 304.2 g/L, respectively. Organic matter was also present in almost every sample of sepiolite (Table 2). Other selected chemical, physical, and physicochemical characteristics of the raw sepiolite were also provided in Table 2.

The X-ray diffraction (XRD) pattern of the raw sepiolite sample (Figure 1) clearly showed that the major component was sepiolite followed by dolomite as confirmed by the IR bands at 1427 and 728 cm^{-1} (Figure 2) in the FTIR spectra (Eren *et al.*, 2010; Lescano *et al.*, 2014). The presence of distinctive sepiolite and dolomite peaks were obvious in the raw sepiolite XRD pattern and indicated a sepiolite with poor
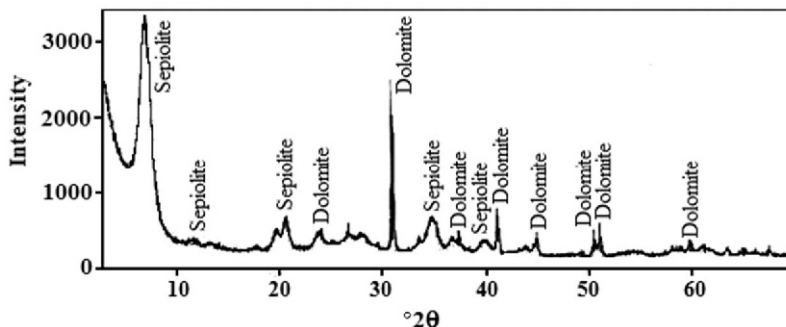

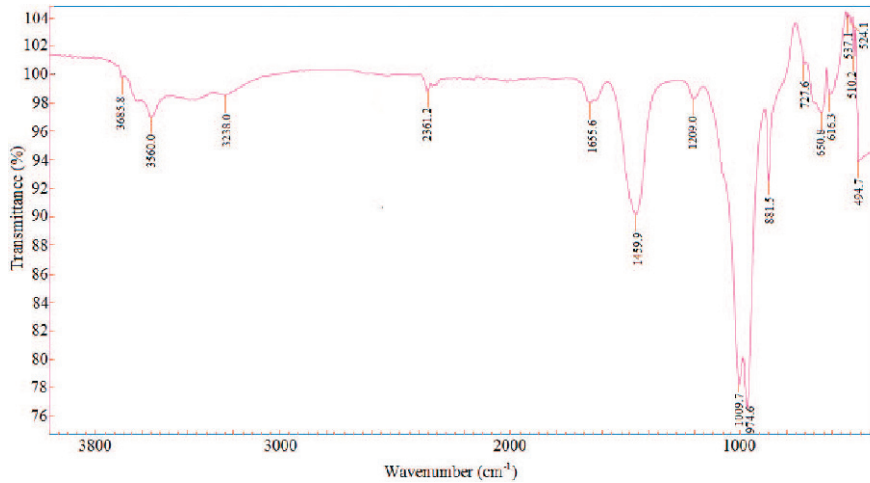Figure 1. X-Ray diffraction pattern of natural sepiolite.

Figure 2. FTIR spectrum of natural sepiolite.

crystallinity. Moreover, the FTIR spectrum of raw sepiolite (Figure 2) differed from a very crystalline and intermediately crystalline sepiolite by the absence of the band at 3720 cm^{-1}, which was assigned to the OH stretching vibration of silanol (Si-OH) groups. Martienssen (2009) suggested that the 3640 cm^{-1} band may arise from limited trioctahedral substitutions and the 3620 cm^{-1} band from structural MgOH dioctahedral stretching modes. The very small band of the triple bridge Mg$_3$OH group in the octahedral sheet at 3685 cm^{-1} was attributed to structural hydroxyls (Martienssen, 2009). The analysis of FTIR spectra as

well as XRD data (Figure 1) showed a relatively high amount of CaO (6.01%) (Table 2), which demonstrates that the sepiolite sample consists mainly of clay and impurities, such as organic matter and dolomite, and suggests that the sepiolite sample used in this study was of moderate quality.

The nitrogen adsorption/desorption isotherm at −196ºC and the cumulative pore volume (Figure 3) and log-differential pore volume distribution curves are shown in Figure 4. The adsorption isotherm of natural sepiolite was of type II according to The International Union of Pure and Applied Chemistry (IUPAC) classi-
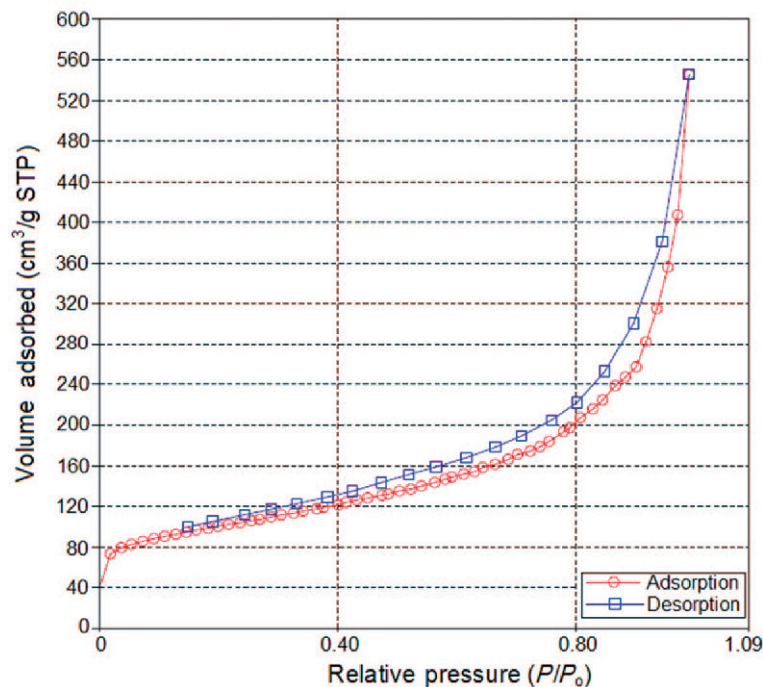

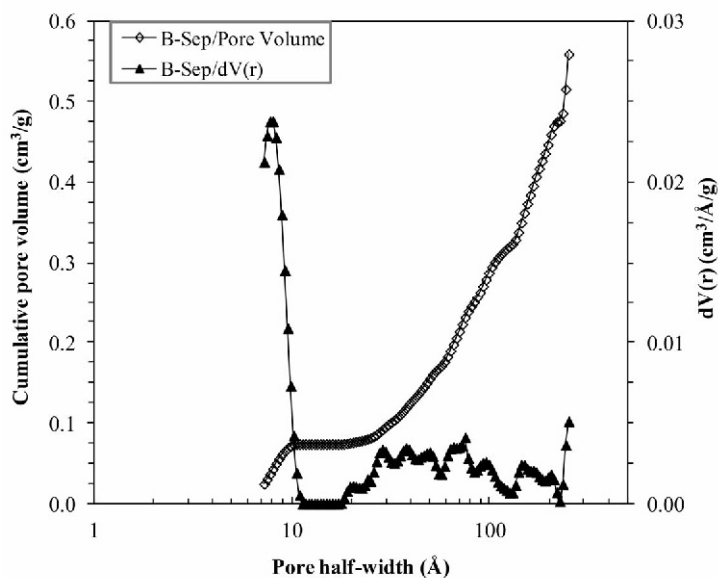Figure 3. N$_2$ adsorption and desorption isotherms at −196ºC for natural sepiolite.

Figure 4. Cumulative pore volume and pore-size distribution curves for natural sepiolite.

fication and showed hysteresis to a certain degree (Broekhoff, 1979; Sing *et al.,* 1985; Shields *et al.*, 2004; Alothman, 2012). A visual inspection of the isotherm shapes indicated that the porous network in the sepiolite sample had micropores, mesopores, and macropores. The total amount of N_2 adsorbed at high relative pressure was 55%. This result indicated a higher porosity, which yielded a greater available volume for N_2 adsorption within the macropores. The N_2 saturation plateau was not parallel to the relative pressure axis and indicated that the sepiolite contained a large proportion of mesopores. This was confirmed from the cumulative pore volume and log-differential pore volume distribution curves (Figure 4). The natural sepiolite had a BET surface area of 358 m^2/g, a pore diameter of 7.26−251.16 Å, and the volume of the 7.26−19.69 Å range of pore sizes was 13.44% of the total pore volume. Moreover, a very sharp peak at a pore half-width of around 8 Å obtained from the 7−251 Å interval (Figure 4) of the log-differential pore volume distribution curve was related to N_2 entry into intracrystalline tunnels and indicates uniform micropores and a multimodal pore size distribution in the sepiolite. The average pore diameter of micro-mesopores determined from the specific micro-mesopore volume and the specific surface area was about 47.2 Å.

The textural features observed by FE-SEM (Figure 5) confirmed that the natural sepiolite has the characteristic fibrous morphology of fiber length, width, curliness, arrangement, and porosity. The fibers were composed of tablets and needle-like structures arranged in parallel (Suárez and García-Romero, 2012) and consisted of intermediate fiber lengths between 1 and 10 μm that were much longer than fiber widths. Semi-quantitative EDX analysis showed that the natural sepiolite was composed mainly of Si and Mg and smaller amounts of Ca and Al.

Adsorption isotherms of pyrene onto natural sepiolite

The adsorption isotherm of pyrene onto natural sepiolite at 25ºC (Figure 6) indicated that pyrene uptake increased sharply when the initial solution concentration was increased from 2 to about 3 mg/L to reach an adsorption capacity of 6 mg/g. This sharp increase in pyrene adsorption was followed by a more gradual increase in adsorption from 6−6.8 mg/L and adsorption leveled off to a maximum value of 8 mg/g. This strong pyrene-sepiolite interaction was confirmed by a very steep slope at low equilibrium concentration values fitting an H-type isotherm behavior, which is a special case of the L-type Langmuir isotherm and usually indicates chemisorption according to the Giles, Smith, and Huitson (1974) classification of adsorption isotherms for solutes in dilute solution. Natural sepiolite effectively removed pyrene at low initial solution concentrations. At higher initial pyrene concentrations, however, adsorption reached a maximum capacity depicted by a plateau. This behavior indicated that few of the readily accessible sites on the sepiolite were available. In other words, a relatively large volume of micropores (pores less than 20 Å) generally corresponded to a large surface area and a large adsorption capacity for small molecules, whereas a large volume of mesopores (20 < d < 500 Å) and macropores (d > 500 Å) is usually directly correlated with the adsorption capacity for large molecules, such as pyrene. Therefore, pyrene adsorption was strongly dependent on the presence of meso/macropores and particularly micropores. The relatively high mesopore and macropore volume of the sepiolite was likely responsible for
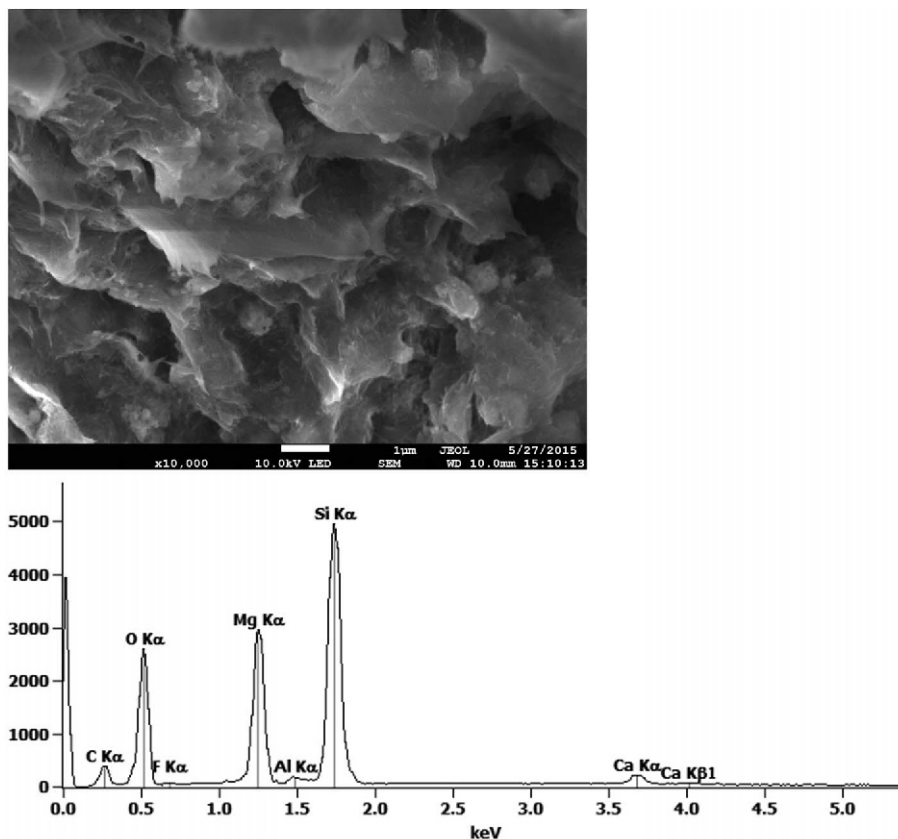
Figure 5. FE-SEM image and semi-quantitative (EDX) analysis of natural sepiolite.

the high adsorption rate constant, which was consistent with the underlying assumption of the importance of vacant sites for a pseudo-second order adsorption
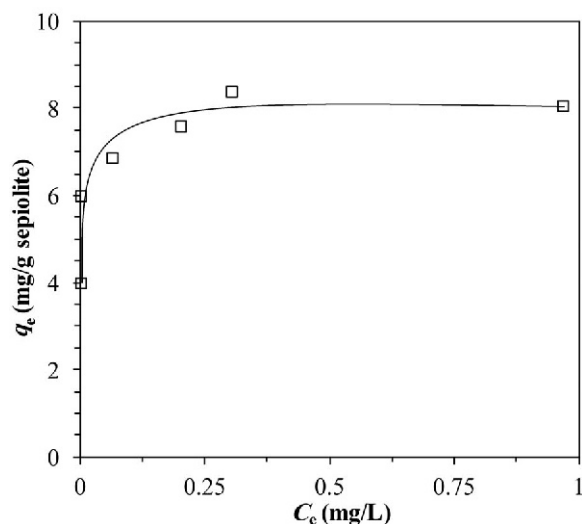

Figure 6. Pyrene adsorption isotherm of natural sepiolite at 25ºC, where C_i range = 2 to 5 mg/L; natural pH = 8.78; conditioning time = 2 h; solid:liquid ratio = 0.5; and (−) = Langmuir fit.

process. This is in agreement with the work of Valderrama *et al.* (2007) who also observed that a more mesoporous adsorbent had about a hundred times greater rate constant than granular activated carbon for the competitive adsorption of PAHs. This implies the possibility that the adsorption rate was mainly controlled by pore-diffusion through the intra-particle pore structure. A similar finding was reported by Cobas *et al.* (2014). They noted that the rates of pyrene adsorption onto sepiolite took place in two stages; the first stage was attributed to boundary layer diffusion and the second linear increase in adsorption reflected the effect of pore diffusion. As such, the pseudo-second order model was based on the adsorption capacity of the adsorbent, *i.e.* the vacant active sites and the adsorption process was driven by chemisorption according to Ho and McKay (2000).

The adsorption isotherms of pyrene on natural sepiolite at three different temperatures (25, 40, and 55ºC) (Figure 7) and the adsorption equilibrium data were analyzed according to the two commonly used isotherm models in this study; the Langmuir and Freundlich isotherms. An increase in the equilibrium adsorption capacity of natural sepiolite (Figure 7) was observed as the temperature was increased by 15ºC, which indicated that pyrene adsorption to sepiolite was
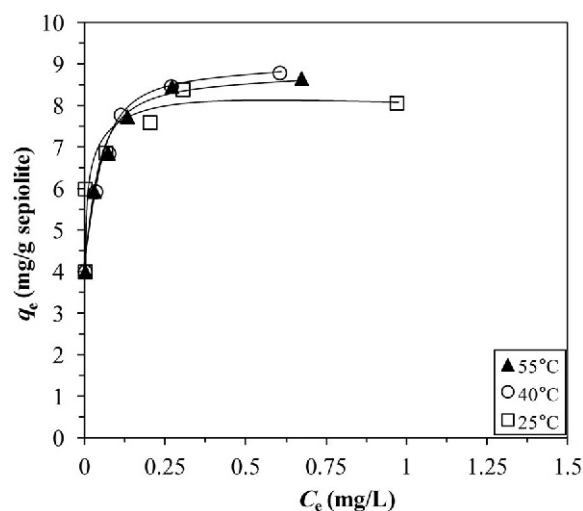
Figure 7. Pyrene equilibrium adsorption isotherms on natural sepiolite at 25, 40, and 55ºC (298, 313, 328 K). The adsorption isotherm conditions were as follows: pyrene C_i = 2 to 5 mg/L; sepiolite natural pH = 8.78; conditioning time = 2 h; solid:liquid ratio = 0.5; fitted line (−) = Langmuir fit.

an endothermic and chemisorption process. In addition, no significant effect of temperature was observed during pyrene adsorption by the sepiolite sample at temperatures above 40 and 55ºC. As expected, the sepiolite/ pyrene system reached equilibrium at low pyrene concentrations at temperatures above 25ºC, which indicated that the K_L values were lower at higher temperatures where pyrene solubility is greater. In an early study, Yu *et al.* (2012) showed that the mole fraction solubility of pyrene in methanol increased with an increase in temperature.

In the sepiolite/pyrene system, the increase in adsorption with increased temperature and the fast pyrene adsorption kinetics and equilibrium (2 h) may suggest that chemisorption was a dominant adsorption mechanism. Nevertheless, this alone was not sufficient to determine the type of adsorption. The type of adsorption may be determined through thermodynamic quantities, such as free energy (ΔG_{ads}^o) of adsorption and the heat of adsorption (ΔH_{ads}^o), both of which can be obtained from the adsorption data.

The Langmuir and Freundlich adsorption isotherm parameters of the pyrene/sepiolite system obtained at temperatures of 25, 40, and 55ºC were determined from the intercepts and slopes of plots of C_e/q_e *vs.* C_e for the Langmuir model and plots of ln q_e *vs.* ln C_e for the Freundlich model (Figure 8a and 8b) for natural sepiolite. The Langmuir and Freundlich model parameters at different temperatures and the correlation coefficients (Table 3) revealed that the pyrene/sepiolite system data fit the Langmuir model ($R^2 > 0.99$) better than the Freundlich model. The Langmuir monolayer adsorption capacity, q_m, did not change much with temperature, but K_L (Table 3) significantly decreased from 153.56 to 81.26 L/mg with increases in temperature. A lower K_L value indicates a higher affinity. This indicates that pyrene adsorption to sepiolite was controlled by an endothermic process.

The free energy values indicate the degree of spontaneity of the sorption process and a higher negative value reflects a more energetically favorable sorption. The ΔH_{ads}^o and ΔS_{ads}^o values were obtained from the slope and intercept of a plot of ln K_d against $1/T$ (Figure 9). The calculated parameters (Table 4) showed that temperature had little effect on the amount of pyrene
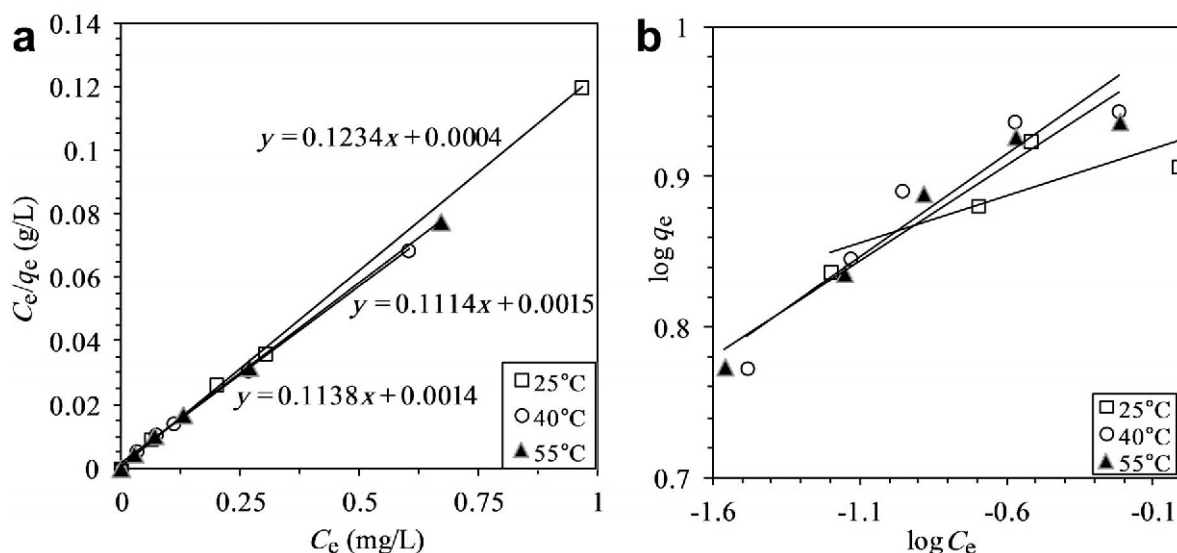

Figure 8. Langmuir (a) and Freundlich (b) isotherm plots for pyrene adsorption to natural sepiolite at 25, 40, and 55ºC. Pyrene adsorption conditions were as follows: pyrene C_i = 2 to 5 mg/L; natural pH = 8.78; conditioning time = 2 h; and solid:liquid ratio = 0.5.

Table 3. Parameters of Langmuir and Freundlich models fitted to the pyrene adsorption to natural sepiolite isotherm data.

Adsorbents	Temperature (ºC)	Langmuir constants			Freundlich constants		
		q_m (mg/g)	K_L (L/mg)	R^2	n	K_F (mg/g) $(L/mg)^{1/n}$	R^2
Natural sepiolite	25	8.10	308.64	0.9994	10.74	8.67	0.8097
	40	8.98	74.24	0.9988	7.29	9.95	0.9031
	55	8.79	81.26	0.9992	7.86	9.64	0.9424

sorbed to natural sepiolite. Activation energies for the sorption process were between 26.3 and 31.2 kJ/mol and clays with larger surface areas gave higher activation energies. These values were characteristic of diffusion controlled processes. Furthermore, the negative values of ΔG^o_{ads} for natural sepiolite (Table 4) indicated the spontaneous nature of the adsorption process with a higher negative value reflecting a more energetically favorable adsorption. The decrease in the negative value of ΔG^o_{ads} with an increase in the temperature indicated that the adsorption of pyrene on the sepiolite became more favorable at higher temperatures. When the values of ΔG^o_{ads} are slightly over −20 kJ/mol and the process is endothermic, the interaction may be defined as a weak chemical bond. The contribution of entropy, $T\Delta S^o_{ads}$, was much higher than the contribution of enthalpy. This clearly revealed that the adsorption reactions in the pyrene/sepiolite system were governed by entropy.

Adsorption mechanism of pyrene onto natural sepiolite

In addition to thermodynamic data, the FTIR spectra (Figure 10) and an analysis of the FE-SEM images (Figure 11) showed that pyrene adsorption to natural sepiolite occurred both in structural channels and to the large number of Si-OH groups. This was due to the large surface area (358 m²/g) of sepiolite on the basal surfaces,
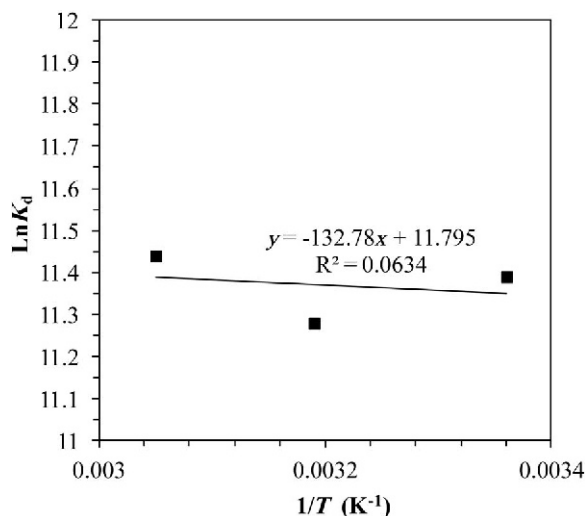

Figure 9. Plots of ln K_d vs. *1/T* for pyrene adsorption onto natural sepiolite at 298, 313, and 328 K.

but the intracrystalline interactions with pyrene were more favorable than the surface Si-OH groups, which can react directly with pyrene to form true covalent bonds (chemical interactions). Pyrene adsorption to sepiolite can be seen to take place on water molecules coordinated to Mg^{2+} cations at the edges of particles in openings and inside the channels. The spectra of natural sepiolite had bands at 3685 cm^{-1} and 3687 cm^{-1} which correspond to Mg−OH vibrations inside sepiolite structural blocks. The bands at 3626 and 3625 cm^{-1} were characteristic for the stretch of MgOH (dioctahedral) and the two bands located at 3560 cm^{-1} and 1655 cm^{-1} were assigned to the vibrations of water coordinated to the Mg^{2+} at the edges of sepiolite structural blocks. The bands at 3685 cm^{-1} (Figure 10) disappeared after pyrene adsorption. This result suggests that Mg^{2+} cations were removed and the water and hydroxyl group coordinated to Mg^{2+} cations were lost during pyrene adsorption to natural sepiolite. The adsorption of pyrene at different concentrations showed that bands in the 3560 cm^{-1} region significantly decreased in intensity and at around 1655 cm^{-1} a small change in wavenumber position occurred which might be related to the interactions between pyrene molecules and natural sepiolite. This confirms that coordinated water molecules mainly located inside the tunnels and/or channels could be involved in hydrogen bonding (water bridges) or could be replaced by pyrene molecules to give rise to the direct coordination of water molecules to Mg^{2+} ions on the borders of structural blocks. This can result in the penetration of the adsorbed pyrene molecules into the structural cavities of the sepiolite. In fact, sepiolite acts as a molecular sieve to separate the adsorbate species by molecular size. In case of the present study, a correlation between the pyrene adsorption capacity and molecular dimensions of pyrene (~9.2 Å) suggests that natural sepiolite, which has a micropore (7−20 Å) volume of 13.36%, acted to a certain degree as a molecular sieve for the large pyrene molecules. Therefore, a greater fraction of the micropores would not be accessible to pyrene. The pyrene was most capable of accessing mesopores that largely control the specific adsorption capacity and adsorption intensity of sepiolite. The dependence of pore volume and surface area on pore size showed that most of the pore surface area, but only a minor fraction of the total pore volume, was associated with the smaller mesopores (>20 Å in diameter). Natural sepiolite has an average pore diameter of about 47.2 Å, but most of the

Table 4. Thermodynamic parameters for sepiolite/pyrene systems at 278, 313, and 328 K.

Adsorbent	ΔS^o (kJ/mol)	ΔH^o (kJ/mol)	ΔG^o (kJ/mol)		
			298 K	313 K	328 K
Natural sepiolite	0.098	1.10	−26.33	−29.35	−31.20

porosity was attributed to the contributions of external pores from inter-fibers/bundle spaces because of the effective diameters of these pores were >15 Å. The FE-SEM images for natural sepiolite (Figure 5) indicated spherical aggregates that consist of bundles of 10−50 nm wide fibrous nanoparticles (García-Romero and Suárez, 2013) a few microns long, whereas the sepiolite nanofibers loaded with pyrene were usually stuck together in bundles of very short fibers <1 μm in diameter. The pyrene adsorbed to natural sepiolite (Figures 11a, 11b) exhibited a fairly straight and rigid fiber arrangement (aggregation of laths to form rods) that depended on the amount of adsorbed pyrene.

CONCLUSIONS

In this study, pyrene adsorption from aqueous media by natural sepiolite was examined as a function of the initial pyrene concentration and temperature. The experimental results showed that the sepiolite effectively removed pyrene at low initial concentrations. However,

at higher concentrations, the isotherm reached a maximum capacity as highlighted by the plateau fitting to only a special case of the L-type Langmuir isotherm. The maximum pyrene adsorption capacity of the sepiolite was measured to be 8.98 mg/g at a temperature of 313 K. The effect of temperature on pyrene adsorption to sepiolite was utilized to calculate, such thermodynamic parameters as the change in free energy of adsorption (ΔG^o_{ads}) and the heat of adsorption (ΔH^o_{ads}). While the free energy of adsorption was calculated to be 26−31 kJ/mol, the heat of adsorption was 1.10 kJ/mol. For the total adsorption energy, the contribution of entropy $T\Delta S^o_{ads}$ was much larger than enthalpy. This clearly revealed that the adsorption reactions in both pyrene/sepiolite systems were governed by entropy.

The FTIR spectra confirmed that pyrene adsorption strongly depends on the interactions with the channels of sepiolite, particularly with the surface Si-OH groups, which can react directly with pyrene to form true covalent bonds (chemical interactions) between sepiolite and pyrene. The FE-SEM images of the sepiolite treated
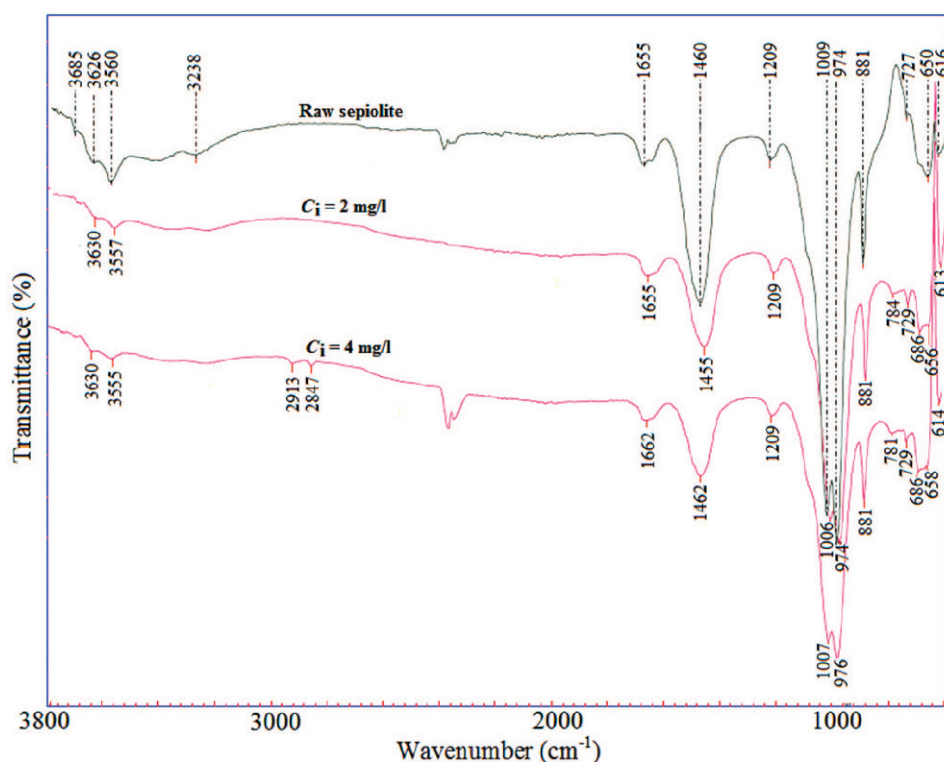

Figure 10. FTIR spectra of natural sepiolite both in raw form and treated with 2 and 4 mg/L pyrene.
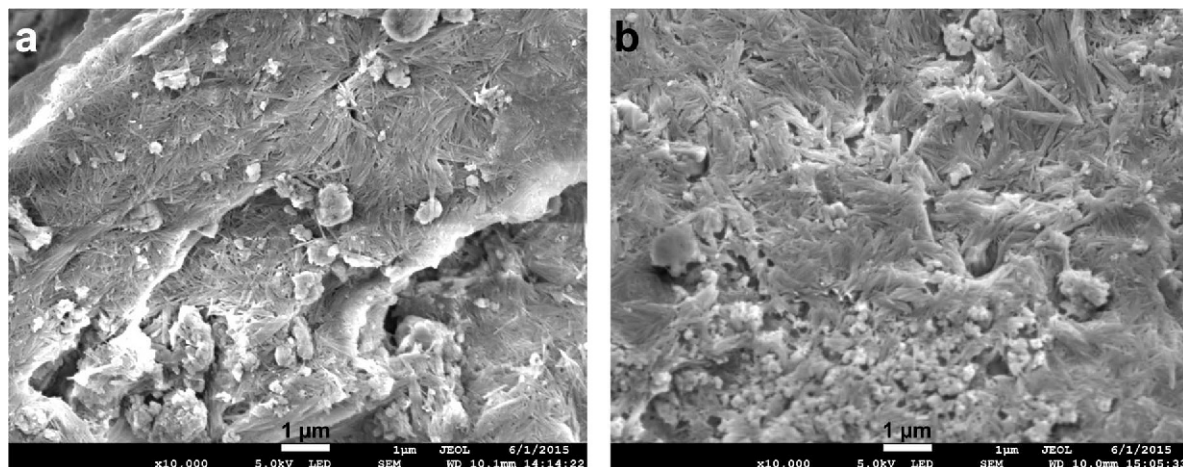
Figure 11. FE-SEM images of the natural sepiolite samples after treatment with (a) 2 mg/L and (b) 4 mg/L pyrene.

with different concentrations of pyrene revealed morphological changes in the sepiolite due to adsorbed pyrene molecules that can be attributed to the aggregation of laths to form rods and thicker bundles.

ACKNOWLEDGMENTS

REFERENCES

Alvarez, A., Santaren, J., Esteban-Cubillo, A., and Aparicio, P. (2011) Current industrial applications of palygorskite and sepiolite. Pp. 281−298 in: *Developments in Palygorskite-Sepiolite Research* (E. Galan and A. Singer, editors). Chapter 12. Elsevier, Amsterdam.

Alothman, Z.A. (2012) A Review: Fundamental aspects of silicate mesoporous materials. *Materials*, **5**, 2874−2902.

Anbia, M. and Moradi, S.E. (2009) Removal of naphthalene from petrochemical wastewater streams using carbon nanoporous adsorbent. *Applied Surface Science*, **255**, 5041−5047.

Ania, C.O., Cabal, B., Pevida, C., Arenillas, A., Parra, J.B., Rubiera, F., and Pis, J.J. (2007) Effects of activated carbon properties on the adsorption of naphthalene from aqueous solutions. *Applied Surface Science*, **253**, 5741−5746.

Broekhoff, J.C.P. (1979) Mesopore determination from nitrogen sorption isotherms: Fundamentals, scope, limitations. *Studies in Surface Science and Catalysis*, **3**, 663−684.

Chang, C.F., Chang, C.Y., Chen, K.H., Tsai, W.T., Shie, J.L., and Chen, Y.H. (2004) Adsorption of naphthalene on zeolite from aqueous solution. *Journal of Colloid and Interface Science*, **277**, 29−34.

Cho, J.Y., Son, J.G., Park, B.J., and Chung, B.Y. (2009) Distribution and pollution sources of polycyclic aromatic hydrocarbons (PAHs) in reclaimed tidelands and tidelands of the western sea coast of South Korea. *Environmental Monitoring and Assessment*, **149**, 385−393.

Cobas, M., Ferreira, L., Sanromán, M.A., and Pazos, M. (2014) Assessment of sepiolite as a low-cost adsorbent for phenanthrene and pyrene removal: Kinetic and equilibrium studies. *Ecological Engineering*, **70**, 287−294.

Crisafully, R., Milhome, M.A.L., Cavalcante, R.M., Silveira,

E.R., Keukeleire, D.D., and Nascimento, R.F. (2008) Removal of some polycyclic aromatic hydrocarbons from petrochemical wastewater using low-cost adsorbents of natural origin. *Bioresource Technology*, **99**, 4515−4519.

Dai, Y., Niu, J., Yin, L., Xu, J., and Xi, Y. (2011) Sorption of polycyclic aromatic hydrocarbons on electrospun nanofibrous membranes: Sorption kinetics and mechanism. *Journal of Hazardous Materials*, **192**, 1409−1417.

Dowaidar, A.M., El-Shahawi, M.S., and Ashour, I. (2007) Adsorption of polycyclic aromatic hydrocarbons onto activated carbon from non-aqueous media: 1. The influence of the organic solvent polarity. *Separation Science and Technology*, **42**, 3609−3622.

EN 1097-3. (1998) *Test for Mechanical and Physical Properties of Aggregates-Part 3: Determination of Loose Bulk Density and Voids*, European Committee for Standardization, Brussels.

Eren, E., Cubuk, O., Ciftci, H., Eren, B., and Caglar, B. (2010) Adsorption of basic dye from aqueous solutions by modified sepiolite: Equilibrium, kinetics and thermodynamics study. *Desalination*, **252**, 88−96.

García-Romero, E. and Suárez, M. (2013) Sepiolite–palygorskite: Textural study and genetic considerations. *Applied Clay Science*, **86**, 129−144.

Giles, C.H., Smith, D., and Huitson, A. (1974) A general treatment and classification of the solute adsorption isotherm. I. Theoretical. *Journal of Colloid and Interface Science*, **47**, 755−765.

Haghseresht, F. and Lu, G.Q. (1998) Adsorption characteristics of phenolic compounds onto coal-reject-derived adsorbents. *Energy Fuels*, **12**, 1100−1107.

Hall, S., Tang, R., Baeyens, J., and Dewil, R. (2009) Removing polycyclic aromatic hydrocarbons from water by adsorption on silicagel. *Polycyclic Aromatic Compounds*, **29**, 160−183.

Ho, Y.S. and McKay, G. (2000) The kinetics of sorption of divalent metal ions onto sphagnum moss peat. *Water Research*, **34**, 735−742.

Hur, J. and Schlautman, M.A. (2006) Humic substance adsorptive fractionation by minerals and its subsequent effects on pyrene sorption isotherms. *Journal Environmental Science Health A*, **41**, 343−358.

Irha, N. (2000) Sorption of pyrene from water by oil shale ash and mineral particles. *Toxicological and Environmental Chemistry*, **74**, 105-110.

Iu, K.-K. and Thomas, J.K. (1990) Photophysical properties of pyrene in zeolites. 2. Effects of coadsorbed water. *Langmuir*, **6**, 471−478.

Kirso, U., Alumaa, P., Irha, N., Petersell, V., Teinemaa, J.S., and Steinnes, E. (2000) Sorption of pyrene to two Estonian soils. *Polycyclic Aromatic Compounds*, **20**, 55–66.

Kojdecki, M.A., Bastida, J., Pardos, P., and Amorós, P. (2005) Crystalline microstructure of sepiolite influenced by grinding. *Journal of Applied Crystallography*, **38**, 888–899.

Laegdsmand, M., Jonge, L.W., Moldrup, P., and Keiding, P.K. (2004) Pyrene sorption to water-dispersible colloids: effect of solution chemistry and organic matter. *Vadose Zone Journal*, **3**, 451–461.

Lemić, J., Tomašević-Čanović, M., Adamović, M., Kovačević, D., and Milićevic, S. (2007) Competitive adsorption of polycyclic aromatic hydrocarbons on organo-zeolites. *Microporous and Mesoporous Materials*, **105**, 317–323.

Lescano, L., Castillo, L., Marfil, S., Barbosa, S., and Maiza, P. (2014) Alternative methodologies for sepiolite defibering. *Applied Clay Science*, **95**, 378–382.

Li, Y., Chen, B., and Zhu, L. (2010) Enhanced sorption of polycyclic aromatic hydrocarbons from aqueous solution by modified pine bark. *Bioresource Technology*, **101**, 7307–7313.

Malik, P.K. (2004) Dye removal from wastewater using activated carbon developed from sawdust: adsorption equilibrium and kinetics. *Journal of Hazardous Materials*, **113**, 81–88.

Marchal, G., Smith, K.E.C., Rein, A., Winding, A., Trapp, S., and Karlson, U.G. (2013) Comparing the desorption and biodegradation of low concentrations of phenanthrene sorbed to activated carbon, biochar and compost. *Chemosphere*, **90**, 1767–1778.

Martienssen, W. (2009) *Magnetic Properties of Non-metallic Inorganic Compounds Based on Transition Elements*. Vol. 27. SpringerVerlag, Berlin, Heidelberg.

Morozzi, D. and Scardazza, F. (1998) Adsorption of carcinogenic benz(a)pyrene on activated sludges. *Journal Environmental Science Health A*, **23**, 169–180.

Murray, H.H. (2007) *Applied Clay Mineralogy: Occurrences, Processing and Applications of Kaolins, Bentonites, Palygorskite, Sepiolite, and Common Clays*, First Edition. Elsevier, Amsterdam.

Newsted, J.L. and Giesy, J.P. (1987) Predictive models for photo-induced acute toxicity of polycyclic aromatic hydrocarbons to daphnia magna strauss (cladocera, crustacea). *Environmental Toxicology and Chemistry*, **6**, 445–461.

Owabor, C.N., Ogbeide, S.E., and Susu, A.A. (2010) Adsorption and desorption kinetics of naphthalene, anthracene, and pyrene in soil matrix. *Petroleum Science and Technology*, **28**, 504–514.

Öztürk, N. and Bektas, T.E. (2004) Nitrate removal from aqueous solution by adsorption onto various materials. *Journal of Hazardous Materials*, **112**, 1550–162.

Pal, D. (2012) Adsorption of polycyclic aromatic hydrocarbons using agricultural wastes-effect of lignin content. Pp. 162–165 in: *2nd International Conference on Chemical, Ecology and Environmental Sciences (ICCEES'2012)*, Bangkok.

Paolis, F. and Kukkonen, J. (1997) Binding of organic pollutants to humic and fulvic acid: influence of pH and the structure of humic material. *Chemosphere*, **34**, 1693–1704.

Perez-Gregorio, M.R., Garcia-Falcon, M.S., Martinez-Carballo, E., and Simal-Gandara, J. (2010) Removal of polycyclic aromatic hydrocarbons from organic solvents by ashes wastes. *Journal of Hazardous Materials*, **178**, 273–281.

Ramirez, N.T. and Cutright, J. (2001) Sorption-desorption of pyrene for Colombia and New Mexico soils. *Polycyclic Aromatic Compounds*, **18**, 273–292.

Sabah, E. and Çelik, M.S. (2002) Adsorption mechanism of quaternary amines by sepiolite. *Separation Science and Technology*, **37**, 3081–3097.

Sabah, E., Turan, M., and Çelik, M.S. (2002) Adsorption mechanism of cationic surfactants onto acid and heat activated sepiolites. *Water Research*, **36**, 3957–3964.

Sener, S. and Zyilmaz, A. (2010) Adsorption of naphthalene onto sonicated talc from aqueous solutions. *Ultrasonics Sonochemistry*, **17**, 932–938.

Shields, J.E., Lowell, S., Thomas, M.A., and Thommes, M. (2004) *Characterization of Porous Solids and Powders: Surface Area, Pore Size and Density*. Kluwer Academic Publisher, Boston, USA.

Sing, K.S.W., Everett, D.H., Haul, R.A.W., Moscou, L., Pierotti, R.A., Rouquerol, J., and Siemieniewska, T. (1985) Reporting physisorption data for gas/solid systems with special reference to the determination of surface area and porosity. *Pure and Applied Chemistry*, **57**, 603–619.

Sun, J.H., Wang, G.L., Chai, Y., Zhang, G., Li, J., and Feng, J.L. (2009) Distribution of polycyclic aromatic hydrocarbons (PAHs) in Henan reach of the Yellow River middle China. *Ecotoxicology and Environmental Safety*, **72**, 1614–1624.

Su, Y.H., Zhu, Y.G., Sheng, H., and Chiou, C.T. (2006) Linear adsorption of nonionic organic compounds from water on to hydrophilic minerals, silica and alumina. *Environmental Science & Technology*, **40**, 6949–6954.

Suárez, M. and García-Romero, E. (2012) Variability of the surface properties of sepiolite. *Applied Clay Science*, **67-68**, 72–82.

Teixeira, S.C.G., Ziolli, R.L., Marques, M.R.C., and Pérez, D.V. (2011) Study of pyrene adsorption on two Brazilian soils. *Water Air Soil Pollution*, **219**, 297–301.

Valderrama, C., Cortina, J.L., Farran, A., Gamisans, X., and Lao, C. (2007) Kinetics of sorption of polyaromatic hydrocarbons onto granular activated carbon and macronet hyper-cross-linked polymers (MN200). *Journal of Colloid and Interface Science*, **310**, 35–46.

Valderrama, C., Gamisans, X., Cortina, J.L., Farrán, A., and de las Heras, F.X. (2008) Evaluation of polyaromatic hydrocarbon removal from aqueous solutions using activated carbon and hyper-crosslinked polymer (Macronet MN200). *Journal of Chemical Technology and Biotechnology*, **84**, 236–245.

Vidal, C.B., Barros, A.L., Moura, C.P., de Lima, A.C.A., Dias, F.S., Vasconcellos, L.C.G., Fechine, P.B.A., and Nascimento, R.F. (2011) Adsorption of polycyclic aromatic hydrocarbons from aqueous solutions by modified periodic mesoporous organosilica. *Journal of Colloid and Interface Science*, **357**, 466–73.

Vučelić, D., Simić, D., Kovačević, O., Dojčinović, M., and Mitrović, M. (2002) The effects of grinding on the physicochemical characteristics of white sepiolite from Golesh. *Journal of the Serbian Chemical Society*, **67**, 197–211.

Wang, J., Chen, Z., and Chen, B. (2014) Adsorption of polycyclic aromatic hydrocarbons by graphene and graphene oxide nanosheets. *Environmental Science & Technology*, **48**, 4817–4825.

Yakout, S.M. and Daifullah, A.A.M. (2013) Removal of selected polycyclic aromatic hydrocarbons from aqueous solution onto various adsorbent materials. *Desalination and Water Treatment*, **51**, 6711–6718.

Yu, Q., Ma, X., and Xu, L. (2012) Determination of the solubility, dissolution enthalpy and entropy of pyrene in different solvents. *Fluid Phase Equilibria*, **319**, 5–8.

Yuan, M., Tong, S., Zhao, S., and Jia, C.Q. (2010). Adsorption of polycyclic aromatic hydrocarbons from water using petroleum coke-derived porous carbon. *Journal of Hazardous Materials*, **181**, 1115–1120.

Zeledón-Toruno, Z.C., Lao-Luque, C., de las Heras, F.X.C., and Sole-Sardans, M. (2007) Removal of polycyclic aromatic hydrocarbons from water using an immature coal (leonardite). *Chemosphere*, **67**, 505−512.

Zhang, J., He, M., and Deng, H. (2009) Comparative sorption of phenanthrene and benzo[α]pyrene to soil humic acids. *Soil and Sediment Contamination*, **18**, 725−738.